

Selection effects in Gamma Ray Bursts correlations: consequences on the ratio between GRB and star formation rates

Dainotti, M. G.^{1,2,3}, Del Vecchio, R.³, Nagataki, S.¹, Capozziello, S.^{4,5,6}

ABSTRACT

Gamma Ray Bursts (GRBs) visible up to very high redshift have become attractive targets as potential new distance indicators. It is still not clear whether the relations proposed so far originate from an unknown GRB physics or result from selection effects. We investigate this issue in the case of the $L_X - T_a^*$ correlation (hereafter LT) between the X-ray luminosity $L_X(T_a)$ at the end of the plateau phase, T_a , and the rest frame time T_a^* . We devise a general method to build mock data sets starting from a GRB world model and taking into account selection effects on both time and luminosity. This method shows how not knowing the efficiency function could influence the evaluation of the intrinsic slope of any correlation and the GRB density rate. We investigate biases (small offsets in slope or normalization) that would occur in the LT relation as a result of truncations, possibly present in the intrinsic distributions of L_X and T_a^* . We compare these results with the ones in Dainotti et al. (2013) showing that in both cases the intrinsic slope of the LT correlation is ≈ -1.0 . This method is general, therefore relevant to investigate if any other GRB correlation is generated by the biases themselves. Moreover, because the farthest GRBs and star-forming galaxies probe the reionization epoch, we evaluate the redshift-dependent ratio $\Psi(z) = (1+z)^\alpha$ of the GRB rate to star formation rate (SFR). We found a

¹Astrophysical Big Bang Laboratory, Riken, 2-1 Hirosawa, Wako, Saitama 351-0198, Japan, maria.dainotti@riken.jp.

²Physics Department, Stanford University, Via Pueblo Mall 382, Stanford, CA, USA, E-mail: mdainott@stanford.edu

³Obserwatorium Astronomiczne, Uniwersytet Jagielloński, ul. Orła 171, 31-501 Kraków, E-mails: delvecchioroberta@hotmail.it, dainotti@oa.uj.edu.pl, mariagiovannadainotti@yahoo.it

⁴Dipartimento di Fisica, Università di Napoli "Federico II", Compl. Univ. di Monte S. Angelo, Edificio G, Via Cinthia, I-80126 Napoli, Italy, E-mail: capozziello@na.infn.it

⁵INFN Sez. di Napoli, Complesso Universitario di Monte S. Angelo, Via Cinthia, Edificio N, 80126 Napoli, Italy

⁶Gran Sasso Science Institute (INFN), viale F. Crispi 7, I-67100 L'Aquila, Italy

modest evolution $-0.2 \leq \alpha \leq 0.5$ consistent with Swift GRB afterglow plateau in the redshift range $0.99 < z < 9.4$.

Subject headings: stars: gamma-ray burst: general, statistics, methods: data analysis.

1. INTRODUCTION

GRBs are the farthest sources, seen up to redshift $z = 9.46$ (Cucchiara et al. 2011), and if emitting isotropically they are also the most powerful, (with $E_{iso} \leq 10^{54} \text{erg s}^{-1}$), objects in the Universe. Notwithstanding the variety of their peculiarities, some common features may be identified by looking at their light curves. A crucial breakthrough in this area has been the observation of GRBs by the Swift satellite, launched in 2004. With the instruments on board, the Burst Alert Telescope (BAT, 15-150 keV), the X-Ray Telescope (XRT, 0.3-10 keV), and the Ultra-Violet/Optical Telescope (UVOT, 170-650 nm), Swift provides a rapid follow-up of the afterglows in several wavelengths with better coverage than previous missions. Swift observations have revealed a more complex behavior of the light curves afterglow (O’Brien et al. 2006; Sakamoto et al. 2007) that can be divided into two, three and even more segments in the afterglows. The second segment, when it is flat, is called plateau emission. A significant step forward in determining common features in the afterglow light curves was made by fitting them with an analytical expression (Willingale et al. 2007), called hereafter W07. This provides the opportunity to look for universal features that could provide a redshift independent measure of the distance from the GRB, as in studies of correlations between GRB isotropic energy and peak photon energy of the νF_ν spectrum, $E_{iso} - E_{peak}$, (Lloyd and Petrosian 1999; Amati et al. 2009), the beamed total energy $E_\gamma - E_{peak}$ (Ghirlanda et al. 2004, 2006), the Luminosity-Variability, L-V (Norris et al. 2000; Fenimore and Ramirez-Ruiz 2000), L- E_{peak} (Yonetoku et al. 2004) and Luminosity- τ lag (Schaefer 2003).

Dainotti et al. (2008, 2010), using the W07 phenomenological law for the light curves of long GRBs, discovered a formal anti-correlation between the X-ray luminosity at the end of the plateau L_X and the rest frame plateau end-time, $T_a^* = T_a^{obs}/(1+z)$, where T_a^* is in seconds and L_X is in erg/s. The normalization and the slope parameters a and b are constants obtained by the D’Agostini fitting method (D’Agostini 2005). Dainotti et al. (2011a) attempted to use the LT correlation as a possible redshift estimator, but the paucity of the data and the scatter prevents from a definite conclusion at least for a sample of 62 GRBs. In addition, a further step to better understand the role of the plateau emission has been made with the discovery of new significant correlations between L_X , and

the mean luminosities of the prompt emission, $\langle L_{\gamma,prompt} \rangle$ (Dainotti et al. 2011b). The LT anticorrelation is also a useful test for theoretical models such as the accretion models, (Cannizzo and Gehrels 2009; Cannizzo et al. 2011), the magnetar models (Dall’Osso et al. 2011; Bernardini et al. 2012a,b; Rowlinson et al. 2010, 2013, 2014), the prior emission model (Yamazaki 2009), the unified GRB and AGN model (Nemmen et al. 2012) and the fireshell model (Izzo et al. 2013). Moreover, Hascoët et al. (2014) and van Eerten (2014b) consider both the LT and the L_X - $\langle L_{\gamma,prompt} \rangle$ correlation to discriminate among several models proposed for the origin of plateau. In Leventis et al. (2014) and in van Eerten (2014a) a smooth energy injection through the reverse shock has been presented as a plausible explanation for the origin of the LT correlation. Furthermore, also other authors were able to reproduce and use the LT correlation to extend it in the optical band (Ghisellini et al. 2009), to extrapolated it into correlations of the prompt emission (Sultana et al. 2012) and to use the same methodology to build an analogous correlation in the prompt (Qi and Lu 2012). Finally, it has been applied as a cosmological tool (Cardone et al. 2009, 2010; Dainotti et al. 2013a; Postnikov et al. 2014). Impacts of detector thresholds on cosmological standard candles have also been considered (Shahmoradi and Nemiroff 2009; Petrosian and Lloyd 1998; Petrosian et al. 1999; Petrosian 2002; Cabrera et al. 2007). However, because of large dispersion (Butler et al. 2010; Yu et al. 2009) and absence of good calibration none of these correlations allow the use of GRBs as good standard candles as it has been done e.g. with type Ia Supernovae. An important statistical technique to study selection effects for treating data truncation in GRB correlations is the Efron and Petrosian (1992) method. Another way to study the same problem in GRB correlations, derived modeling the high-energy properties of GRBs, have been reported in Butler et al. (2010). In the latter paper it has been shown that well-known examples of these correlations have common features indicative of strong contamination by selection effects. We compare this procedure with the method introduced by Efron & Petrosian (1992) and applied to the LT correlation (Dainotti et al. 2013b). The paper is organized as follows: section 2 introduces the relation between GRB and SFR, section 2.1 is dedicated to the analysis of a GRB scaling relation, in particular we consider the LT correlation as an example, but the procedure described can be adopted for any other correlation. In section 3 we describe how to build the GRB samples, in section 4 we analyze the redshift evolution of the slope and normalization of the LT correlation. In section 5 we study the selection effects related to simulated samples assuming different normalization and slope values. Then, in section 6 we draw conclusions on the intrinsic slope of the LT correlation and on the evaluation of the redshift-dependent ratio between GRB and star formation rates.

2. The relation between GRB rate and the star formation rate

In order to understand the relation between GRBs and the star formation, it is often assumed that the GRB rate (RGRB) is proportional to the SFR then the predicted distribution of the GRB redshift is compared to the observed distribution (Totani 1997; Mao and Mo 1998; Wijers et al. 1998; Porciani and Madau 2001; Natarajan et al. 2005; Jakobsson et al. 2006; Daigne and Mochkovitch 2007; Le and Dermer 2007; Coward 2007; Mao 2010). However, this relationship is not an easy task to handle, because some studies show that GRBs do not seem to trace the star formation unbiasedly (Lloyd and Petrosian 1999). Namely, the ratio between the RGRB and SFR, RGRB/SFR, increases with redshift (Kistler et al. 2008; Yüksel and Kistler 2007) significantly. This means that GRBs are more frequent for a given star formation rate density at earlier times. In fact, while observations consistently show that the comoving rate density of star formation is nearly constant in the interval $1 \leq z \leq 4$ (Hopkins and Beacom 2006), the comoving rate density of GRBs appears evolving distinctly. In our approach we explicitly take into consideration this issue when we fit the observed GRB rate with the model. Selection effects involved in a GRB sample are of two kinds : the GRB detection and localization; and the redshift determination through spectroscopy and photometry of the GRB afterglow or the host galaxy. These problems have been object of extensive study in literature (Bloom 2003; Fiore et al. 2007; Guetta and Della Valle 2007). Moreover, the Swift trigger, is very complex and the sensitivity of the detector is very difficult to parameterize exactly (Band 2006), but in this case not dealing with prompt peak energy we do not have to take into consideration the double truncation present in data (Lloyd and Petrosian 1999). In the case of plateau it is easier, since an effective luminosity threshold appears to be present in the data which can be approximated by a 0.3 – 10 keV energy flux limit $F_{lim} \equiv 2 \times 10^{12} \text{ erg cm}^2 \text{ s}^{-1}$ (Dainotti et al. 2013b). The luminosity threshold is then $L_{lim} = 4\pi D_L^2(z, \Omega_M, H_0) F_{lim}$, where D_L is the luminosity distance to the burst. Throughout the paper, we assume a flat universe with $\Omega_M = 0.28$, $\Omega_\lambda = 0.72$ and $H_0 = 70 \text{ km s}^{-1} \text{ Mpc}^{-1}$. In our approach below several models are considered and then the one that best matches the GRB rate with star formation rate has been chosen.

2.1. GRBS WORLD MODEL

We derive a model capable of reproducing the observed Swift GRB rate as a function of redshift, luminosity and time of the plateau emission. Rest frame time and luminosity at the end of the GRB plateau emission show strong correlations as discovered by Dainotti et al. (2008) and later updated by Dainotti et al. (2010, 2011a,b, 2013a). Therefore, all these quantities must be considered in deriving reliable rates.

We characterize the GRB rate as a product of terms involving the redshift z of the bursts, the isotropic equivalent luminosity release (0.3-10 keV) L_X and the duration T_a^* .

Let us assume that a scaling relation exists so that the luminosity $L_X(T_a)$ for a GRB with time scale T_a^* at redshift z is given by :

$$\lambda = \alpha_0 + \alpha_\tau \tau + \alpha_\zeta \zeta \quad (1)$$

where we have introduced the compact notation

$$\begin{cases} \lambda = \log L_X(T_a^*) \\ \tau = \log [T_a^*/(1+z)] \\ \zeta = \log (1+z). \end{cases} \quad (2)$$

and the term ζ accounts for redshift evolution. The luminosity is normalized by the unit of 1 erg s^{-1} and the time by the unit of 1 s, so that non dimensional quantities are considered. All the observables in this model are computed in the rest frame, because we are testing the role played by selection effects in the rest frame, being the LT correlation rest frame corrected. Independently, on the physical interpretation of this relation, (in fact, there are several models that can reproduce it as we have mentioned in the introduction) we can nevertheless expect GRBs to follow Equation 1 with a scatter σ_λ . Moreover, the zero point α_0 may be known only up to a given uncertainty σ_α . Following the approach of Butler et al. (2010) applied for prompt correlations, we assume that λ can be approximated by Gaussian distribution with mean λ_0 , expressed in Equation 1, and the variance σ_{int} as the intrinsic scatter of the correlation. We also write the probability that a GRB with given (τ, ζ) values has a luminosity λ as follows:

$$P_\lambda(\lambda, \tau, \zeta) \propto \exp\left[-\frac{1}{2}\left[\frac{\lambda - (\alpha_0 + \alpha_\tau \tau + \alpha_\zeta \zeta)}{\sigma_{int}}\right]^2\right] \quad (3)$$

with $\sigma_{int}^2 = \sigma_\lambda^2 + \sigma_\alpha^2$, with σ_α the uncertainty of the α_0 value and σ_λ the uncertainty on the luminosity value.

The approximation of a Gaussian distribution both for the luminosity and time is motivated by the goodness of the fit which gives a probability $P = 0.46$ and $P = 0.61$ respectively, see Fig. 1 and 2. We note that the mean, (indicated with $\langle \rangle$) $\langle T_a \rangle = 3.35$ (s) with a variance $\sigma_{T_a} = 0.77$ (s) and $\langle L_X \rangle = 48.04$ (erg/s) with a variance $\sigma_{L_X} = 1.37$ (erg/s) are represented respectively in Fig. 1 and 2.

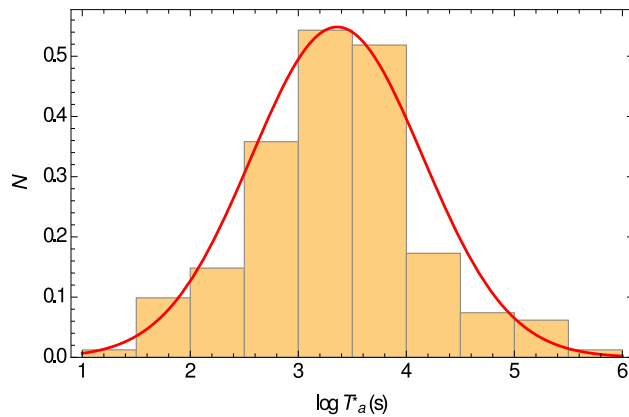


Fig. 1.— Probability Density Distribution of T_a^* , the rest frame end time of the plateau, for GRBs observed from 2005 January until 2014 July analyzed following the Dainotti et al. (2013a) approach with a superimposed best fit of the Gaussian distribution.

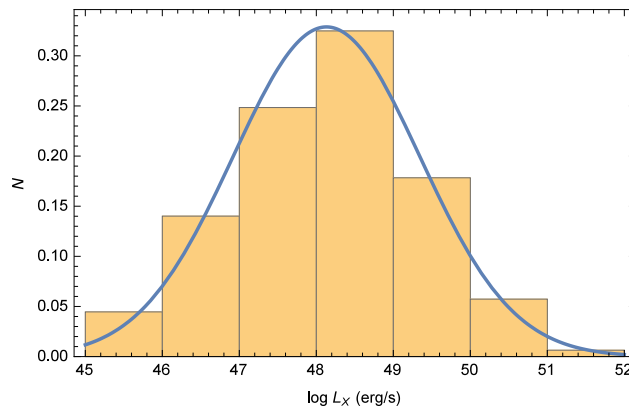


Fig. 2.— Probability Density Distribution of $L_X(T_a)$ at the end of the plateau for GRBs observed from 2005 January until 2014 July analyzed following the Dainotti et al. (2013a) approach with a superimposed best fit of the Gaussian distribution.

In order to obtain the number of GRBs with a given luminosity λ , we need to integrate over the distributions of τ and ζ . We will assume, for simplicity, that τ follows a truncated Gaussian law.

$$P_\tau(\tau) \propto \begin{cases} \exp[-\frac{1}{2}(\frac{\tau-\tau_0}{\sigma_\tau})^2] & \tau_L < \tau < \tau_U \\ 0 & \tau \leq \tau_L \text{ or } \tau \geq \tau_U \end{cases} \quad (4)$$

where τ_L and τ_U indicate respectively the lower limit and upper limit of the observed τ distribution and τ_0 is the mean value of this distribution. The limits of τ are taken from an updated sample of T_a^* composed of 176 GRBs afterglows, with firm redshift determination, from January 2005 till July 2014. The analysis follows the criteria adopted in Dainotti et al. (2013a).

If we assume that the GRBs trace the cosmic star formation rate, we can model their redshift distribution following Butler et al. (2010) as:

$$P_z(z) \propto \frac{\dot{\rho}_*(z) dV}{1+z dz} \quad (5)$$

where $\dot{\rho}_*(z)$ is the comoving GRB rate density, V is the universal volume, and the factor $(1+z)$ accounts for cosmic time dilatation and

$$\frac{dV}{dz} \propto \frac{r^2(z)}{E(z)} \quad (6)$$

with $r(z)$ the comoving distance and $E(z) = H(z)/H_0$ the Hubble parameter normalized to its present day value.

Collecting the different terms, we can finally write the true, detector-independent event \mathcal{N} differential rate, for z , $\log T_a^*$ and $\log L_X$, as:

$$\frac{d\mathcal{N}}{d\lambda d\tau dz} \propto \Psi(z) P_\lambda(\lambda, \tau, \zeta) P_\tau(\tau) P_z(z). \quad (7)$$

We here note that we have introduced the term of the evolution in redshift, $\Psi(z) = (1+z)^\alpha$, following the approach of Lloyd & Petrosian (1999), Dermer (2007) and Robertson & Ellis (2012). In Dermer (2007) assuming that the emission properties of GRBs do not change with time, they find that the Swift data can only be fitted if the comoving rate density of GRB sources exhibits positive evolution to $z > 3 - 5$. In our approach we introduce evolution starting from $z \geq 0.99$.

So using the above expression for P_τ , we find that the number of GRBs with luminosity in the range $(\lambda, \lambda + d\lambda)$ and redshift between z and $z + dz$ is:

$$\frac{d\mathcal{N}}{d\lambda dz} \propto \Psi(z) \frac{\dot{\rho}_*(z)(dV/dz)}{1+z} \frac{\mathcal{F}_{\tau_U} - \mathcal{F}_{\tau_L}}{\sqrt{8\pi\sigma_\tau^2}} \exp\left[-\frac{1}{2} \left[\frac{\lambda - (\alpha_0 + \alpha_\tau\tau + \alpha_\zeta\zeta)}{\sqrt{\sigma_{int}^2}} \right]^2\right] \quad (8)$$

where \mathcal{F}_{τ_U} and \mathcal{F}_{τ_L} are the error functions¹ of the lower and upper limit of the time distribution. Note that Equation 8 is defined up to an overall normalization constant which can be solved by imposing that the integral of $d\mathcal{N}/d\lambda dz$ over (λ, z) gives the total number of observed GRBs. Actually, this is not known since we do not observe all GRBs, but only those passing a given set of selection criteria. However, we will be only interested in the fraction of GRBs in a cell in the 2D (λ, z) space so that we do not need this quantity.

We are aware that we don't map out the true LT relation given selection effects and the observed LT relation. Doing this would require modeling the selection of the GRB sample itself (using the gamma ray threshold) and also seeking to understand the tie between the GRB flux and the afterglow L_X . However, the relation between flux and L_X has been already studied by Dainotti et al. (2013a) and reported briefly in the previous section. Here we computed the new limit related to the updated sample, as it has been shown in the middle panel of Fig 3.

3. SIMULATING THE GRB SAMPLES

The GRBs rate given by Equation 8 has been derived by implicitly assuming that all the GRBs can be detected notwithstanding their observable properties. This is actually not the case. As an example, we will consider hereafter the LT correlation although the formalism and the method we will develop can be easily extended to whatever scaling law. For the LT case, there are two possible selection effects. First, each detector has an efficiency which is not the same for all the luminosities. Only GRBs with $\lambda > \lambda_L$, where λ_L is the lowest detectable luminosity for a given instrument, can be detected while all the GRBs with λ larger than a threshold luminosity λ_U will be found.

Moreover, it is likely that the efficiency of the detector is not constant, but is rather a

¹We remind that the usual definition of the error function is

$$erf(x) = \frac{2}{\sqrt{\pi}} \int_0^x e^{-t^2} dt. \quad (9)$$

function of the luminosity. We will therefore introduce an efficiency function $\mathcal{E}_\lambda(\lambda)$ whose functional expression is not known in advance, but can only take values in the range (0,1). A second selection effect is related to the time duration of the GRB. Indeed, in order to be included in the sample used to calibrate the LT correlation, the GRB afterglow has to be measured over a sufficiently long time scale to make possible to fit the data and extract the relevant quantities. If τ is too small, as it has been shown in Dainotti et al. (2013a) the minimum rest frame time is 14 s, few points will be available for the fit, while, on the contrary, large τ values will give rise to afterglow light curves which could be well sampled by the data. Again, we can parametrize these effects introducing a second efficiency function $\mathcal{E}_\tau(\tau)$ so that the final observable rate is the following:

$$\frac{dN_{obs}}{d\lambda dz} \propto \frac{dN}{d\lambda dz} \times \mathcal{E}_\lambda(\lambda)\mathcal{E}_\tau(\tau). \quad (10)$$

We point out that our formulation, which takes into account of the efficiency functions $\mathcal{E}_\lambda(\lambda)$ and $\mathcal{E}_\tau(\tau)$ in the final observed GRB rate is similar to the approach by Robertson & Ellis (2012) in Equation 1, in which the additional factor K is presented. K is equivalent to our $\mathcal{E}_\lambda(\lambda)$ and $\mathcal{E}_\tau(\tau)$.

It is worth noting that Equation 10 is actually still a simplified description. Indeed, it is in principle possible that other selection effects take place involving observable quantities not considered here, as for example β and the redshift. However, these parameters enter in the determination of λ so that one can (at least in a first order approximation) convert selection cuts on them in a single efficiency function depending only on λ (for the dependence of the flux on the redshift see left panel of Fig. 3). However, as we can see from Fig. 3 β is constant with redshift, and there is no correlation between those two quantities, in fact the Spearman correlation coefficient is $\rho = -0.062$. Nevertheless, Equation 10 provides a

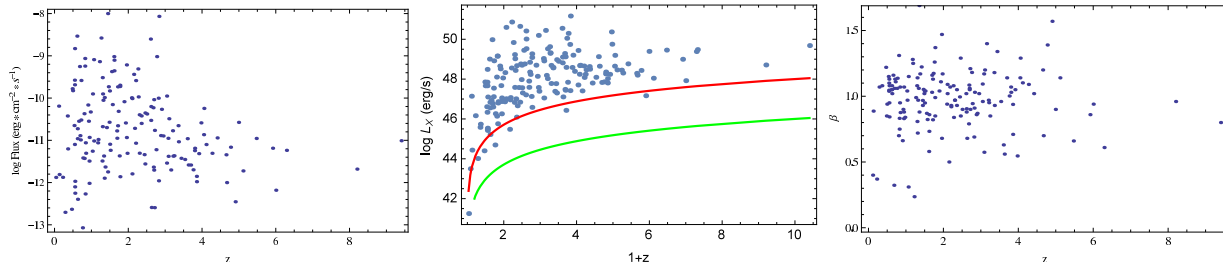


Fig. 3.— Flux at the end of the plateau phase, $\text{Flux}(T_a)$, (left panel) and the spectral index, β , (right panel) as a function of redshift. The limiting luminosity, $\log L_X$ vs $1+z$ shows (middle panel) two lines, one for the limiting flux, $F_{Swift,lim} = 10^{-14} \text{ erg cm}^{-2} \text{ s}^{-1}$ and the other one is the most suitable for a plateau duration of 10^4 s, which is $2 \times 10^{-12} \text{ erg cm}^{-2} \text{ s}^{-1}$.

reasonably accurate description of the observable GRB rate.

In order to evaluate Equation 10 there are different quantities to determine. First, we need to set the scaling coefficients (α_0 , α_τ , α_ζ) and the intrinsic scatter σ_{int} . Second, the mean and variance of the τ distribution (τ_0, σ_τ) has to be given. Finally, an expression for the cosmic SFR $\dot{\rho}_*(z)$ has to be assigned. None of these quantities is actually available. In principle, one could assume a SFR law and fit for the model parameters to a large enough GRBs sample with measured (λ , τ , ζ) values. To this end, one should know the selection function $\mathcal{E}_\lambda(\lambda)\mathcal{E}_\tau(\tau)$ which is not the case. Studies of how light curves would appear to a gamma-ray detector here on Earth have been performed (Kocevski and Petrosian 2013). In this paper the prompt emission pulses are investigated and the conclusion is that even a perfect detector that observes over a limited energy range would not faithfully measure the expected time dilation effects on a GRB pulse as a function of redshift.

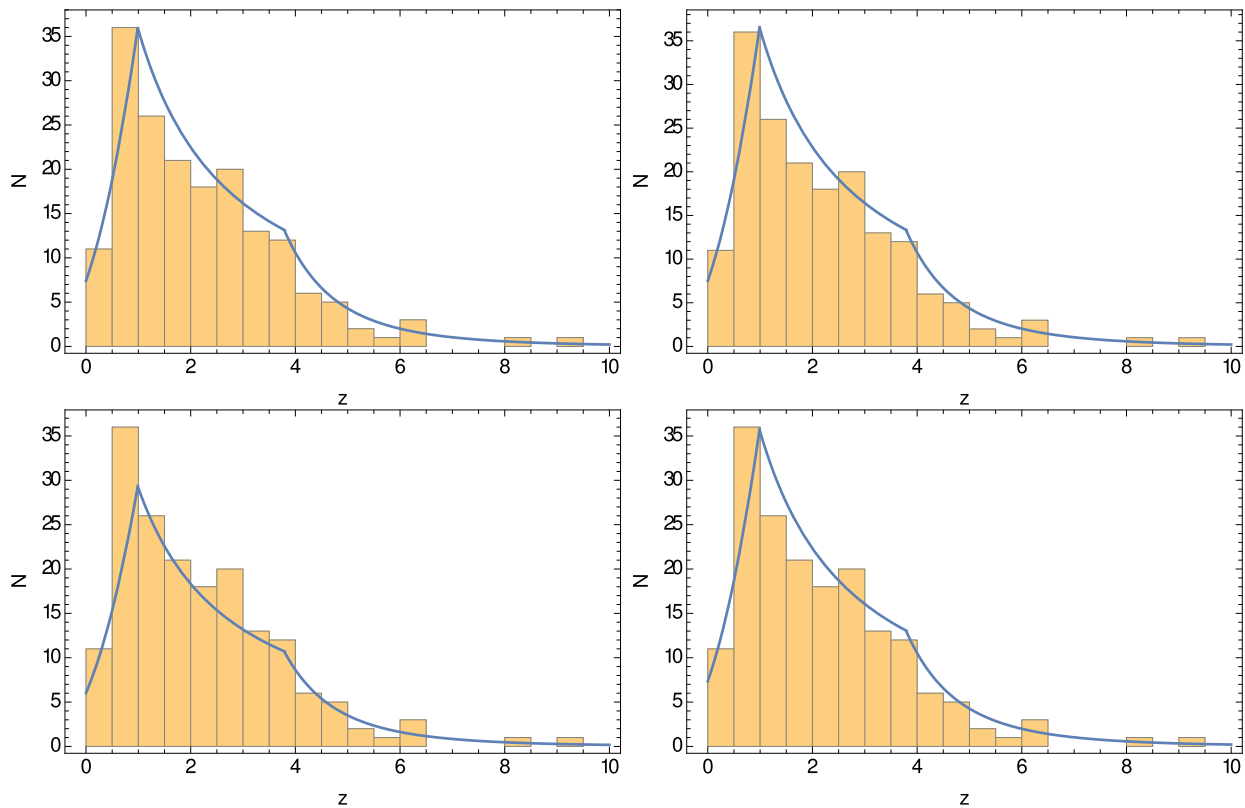


Fig. 4.— GRBs rate density using method of Li (2008) and the observed GRBs rate density obtained by the linear efficiency functions (upper panel), and the polynomial efficiency function (lower panel) with the redshifts distribution of our data sample.

Nevertheless, here we study detector threshold effects on afterglow properties. Our

aim is to investigate how the ignorance of the efficiency function bias the estimate of the correlation coefficients. We can therefore rely on simulated samples based on a realistic intrinsic rate. We proceed as schematically outlined below.

- (i) We assume that the available data represent reasonably well the intrinsic τ distribution so that we can infer (τ_0, σ_τ) from the data themselves. We set $\tau_{L,U} = \tau_0 \pm 5\sigma_\tau$ thus symmetrically cutting the Gaussian distribution at its extreme ends.
- (ii) Based on the shape of the cosmic SFR (Hopkins and Beacom 2006), we assume a broken power law for the comoving GRB rate density:

$$\dot{\rho}_*(z) \propto \begin{cases} (1+z)^{g_0} & z \leq z_0 \\ (1+z)^{g_1} & z_0 \leq z \leq z_1 \\ (1+z)^{g_2} & z \geq z_1 \end{cases} \quad (11)$$

where the relative normalizations are set so that $\dot{\rho}_*(z)$ is continuous at $z_0 = 0.97$ and z_1 and $(z_0, z_1) = (0.97, 4.50)$, $(g_0, g_1, g_2) = (3.4, -0.3, -8.0)$. Moreover, besides the equation 11, we employed other shapes of the SFR (Li 2008; Robertson and Ellis 2012; Kistler et al. 2013) to obtain the observed GRBs rate density. The one used by (Li 2008) is:

$$\dot{\rho}(z) = a + b \times \text{Log}(1+z). \quad (12)$$

The a and b parameters are :

$$(a, b) = \begin{cases} (-1.70, 3.30) & z \leq 0.993 \\ (-0.727, 0.0549) & 0.993 \leq z \leq 3.80 \\ (2.35, -4.46) & z \geq 3.80 \end{cases} \quad (13)$$

Robertson & Ellis (2012) defined the SFR as:

$$\dot{\rho}(z) = \frac{a + b(z/c)^f}{1 + (z/c)^d} + g, \quad (14)$$

where they have $a = 0.009 M_\odot \text{yr}^{-1} \text{Mpc}^{-3}$, $b = 0.27 M_\odot \text{yr}^{-1} \text{Mpc}^{-3}$, $c = 3.7$, $d = 7.4$, and $g = 10^{-3} M_\odot \text{yr}^{-1} \text{Mpc}^{-3}$.

Instead, Kistler et al. (2013) defined the SFR as :

$$\dot{\rho}(z) = \dot{\rho}_0 \times \left[(1+z)^{a\psi} + \left(\frac{1+z}{B} \right)^{b\psi} + \left(\frac{1+z}{C} \right)^{c\psi} \right]^{\frac{1}{\psi}}, \quad (15)$$

with slopes $a = 3.4$, $b = -0.3$, and $c = -2.5$, breaks at $z_1 = 1$ and $z_2 = 4$ corresponding to $B = (1+z_1)^{1-\frac{a}{b}} \sim 5160$ and $C = (1+z_1)^{\frac{(b-a)}{c}} \times (1+z_2)^{\frac{(1-b)}{c}} \sim 11.5$, and $\psi = -10$. Finally, we compare the fitted functions obtained with these four methods with our data distribution. The most reliable fits for our parameters is the SFR used by Li (2008), see Fig. 4 where the best fit among linear (upper panel) and polynomial (lower panel) $\epsilon(\lambda)$ functions are considered. Moreover, we adopted the constraints for the redshift dependent ratio between SFR and GRB rate adopted by Robertson & Ellis (2012). In this paper a modest evolution (e.g., $\Psi(z) \approx (1+z)^\alpha$) with $-0.2 \leq \alpha \leq 1.5$, where the peak probability occurs for $\alpha \approx 0.5$ is consistent with the long GRB prompt data ($P \approx 0.9$). These values can be explained if GRBs occur primarily in low-metallicity galaxies which are proportionally more numerous at earlier times. We note that in our approach we assumed no evolution at low redshift for $z \leq 0.99$ consistently with the posterior probability in Robertson & Ellis (2012) in which no evolution is possible at the $2\text{-}\sigma$ level. However, because a constant $\Psi(z)$ is also ruled out (Robertson and Ellis 2012), then we fit the normalization parameters and the evolution factors obtaining $\Psi(z) \approx (1+z)^{-0.2}$ for $0.993 \leq z \leq 3.8$ and $\Psi(z) \approx (1+z)^{0.5}$ for $z \geq 3.8$. These values of the evolution are compatible with Robertson et al. (2012). Regarding the observed GRB rate we obtained that the best efficiency functions are possible both for two polynomial and two linear as we show in Fig. 4. Table 1 and 2 show the probability that the density rate match the afterglow plateau GRB rate assuming those efficiency functions

- (iii) For given $(\alpha_0, \alpha_\tau, \alpha_\zeta, \sigma_{int})$ values, we divide the 2D space (λ, z) in \mathcal{M} cells and, for each cell, compute the fraction of GRBs in it as:

$$f_{sim}(\lambda_i, z_i) = \frac{\int_{\lambda_i-\Delta\lambda}^{\lambda_i+\Delta\lambda} d\lambda \int_{z_i-\Delta z}^{z_i+\Delta z} dz \frac{dN}{d\lambda dz}}{\int_{\lambda_{min}}^{\lambda_{max}} d\lambda \int_{z_{min}}^{z_{max}} dz \frac{dN}{d\lambda dz}} \quad (16)$$

where we set

$$(\lambda_{min}, \lambda_{max}) = (42.0, 52.0), (z_{min}, z_{max}) = (0, 10). \quad (17)$$

We find more efficient to change variable from z to ζ when dividing the 2D space in 10×10 square cells.

- (iv) For each given cell, we generate $\mathcal{N}_{ij} = f_{sim}(\lambda_i, \zeta_j) \times \mathcal{N}_{sim}$ GRBs (with \mathcal{N}_{sim} the total number of objects to simulate) by randomly sampling (λ, ζ) within the cell boundaries and computing τ by solving Eq. 1.

- (v) To take into account of the selection effects, for each GRB, we generate two random numbers (u_τ, u_λ) uniformly sampling the range $(0, 1)$ and only retain the GRB if $u_\tau \leq \mathcal{E}_\tau(\tau)$ and $u_\lambda \leq \mathcal{E}_\lambda(\lambda)$. Note that, as a consequence of this cut, the final number \mathcal{N}_{obs} of observed GRBs is smaller than the input one \mathcal{N}_{sim} .
- (vi) Finally, for each one of the \mathcal{N}_{obs} selected GRBs, we generate new $(\tau_{obs}, \lambda_{obs})$ values extracting from Gaussian distributions centered on the simulated (τ, λ) values and with a 1% variance. We also associate to each GRB an error set in such a way to be similar to what is actually obtained for GRBs having comparable (τ, λ) values.

The above procedure allows us to build simulated GRBs sample taking into account both the intrinsic properties of any scaling relation and the selection effects induced by the instrumental setup. Moreover, we have referred to an actual GRBs sample in order to set both the limits on (τ, ζ, λ) and the typical measurement errors. Therefore, we can rely on these simulated samples to investigate the impact of selection effects on the recovered slope and intrinsic scatter of the given correlation. To this end, the last ingredient we need is a functional expression for the efficiency functions. Since these are largely unknown, we are forced to make some arbitrary guess. Therefore, we consider two different cases. First, we assume that there is no selection on τ , i.e. we set $\mathcal{E}_\tau = 1$. Two functional expressions are then used for \mathcal{E}_λ , namely a power law:

$$\mathcal{E}_\lambda(\lambda) = \begin{cases} 0 & \lambda < \lambda_L \\ \left(\frac{\lambda - \lambda_L}{\lambda_U - \lambda_L}\right)^{\varepsilon_\lambda} & \lambda_L \leq \lambda \leq \lambda_U \\ 1 & \lambda > \lambda_U \end{cases} \quad (18)$$

and a fourth order polynomial, i.e. :

$$\mathcal{E}_\lambda(\lambda) = \begin{cases} 0 & \lambda < \lambda_L \\ \frac{\varepsilon_1 \tilde{\lambda} + \varepsilon_2 \tilde{\lambda}^2 + \varepsilon_3 \tilde{\lambda}^3 + \varepsilon_4 \tilde{\lambda}^4}{\varepsilon_1 + \varepsilon_2 + \varepsilon_3 + \varepsilon_4} & \lambda_L \leq \lambda \leq \lambda_U \\ 1 & \lambda > \lambda_U \end{cases} \quad (19)$$

with $\tilde{\lambda} = (\lambda - \lambda_L)/(\lambda_U - \lambda_L)$. We try different arbitrary choices for the parameters entering both expressions of \mathcal{E}_λ in order to investigate to which extent the results depend on the exact choice of the efficiency function, see Fig. 5. In a second step, we abandon the assumption $\mathcal{E}_\tau = 1$, to assume for it the same functional expression used for \mathcal{E}_λ , with the same choices for the parameters, but different upper and lower limits depending on τ_U and

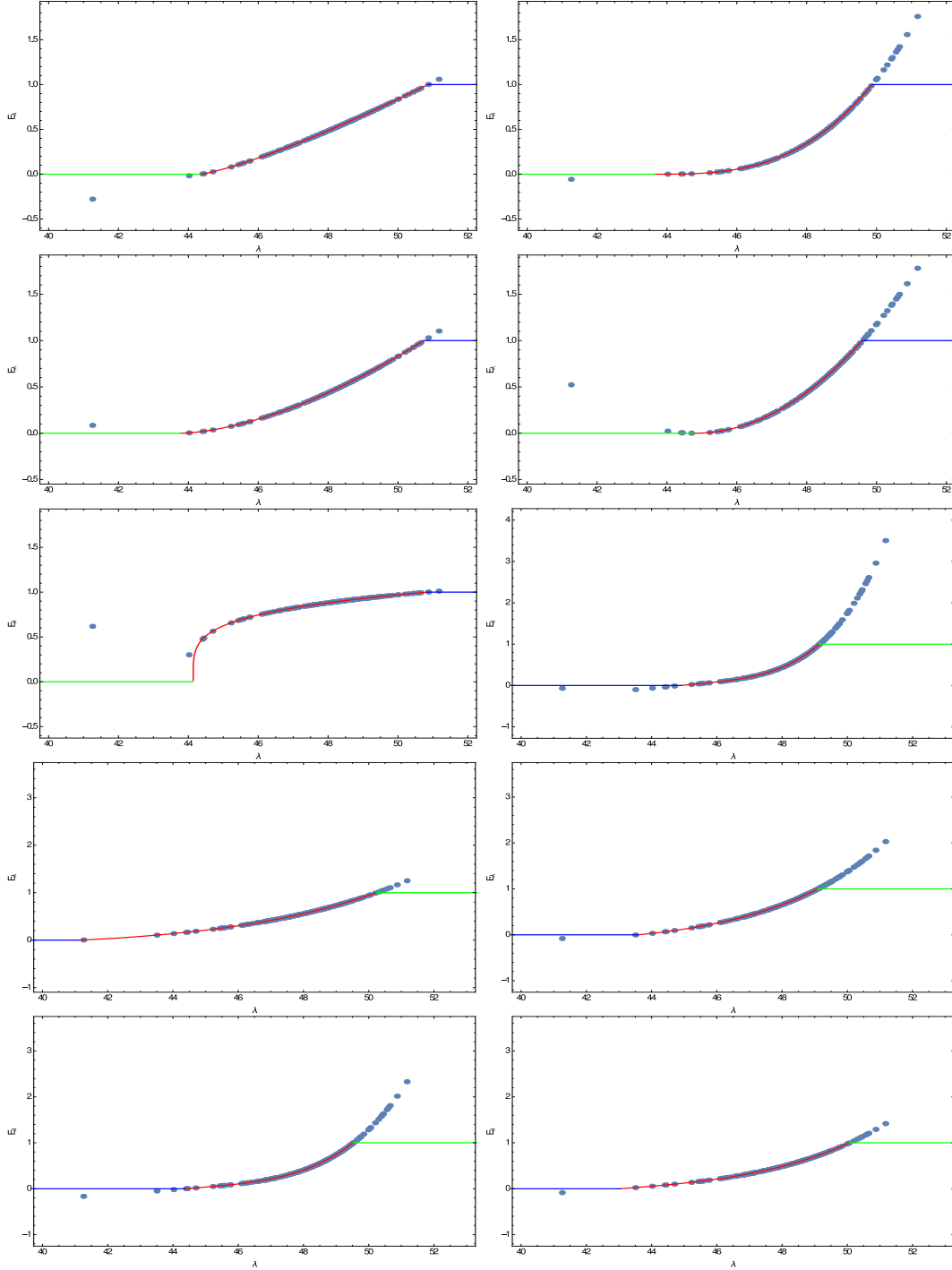


Fig. 5.— The first 5 panels represent examples of the efficiency function for the linear case versus luminosities of the GRBs, λ , in our data sample, while the last 5 panels the efficiency functions for the fourth order polynomial. The linear functions as well the polynomial ones are computed according to Eq. 18, and Eq. 19.

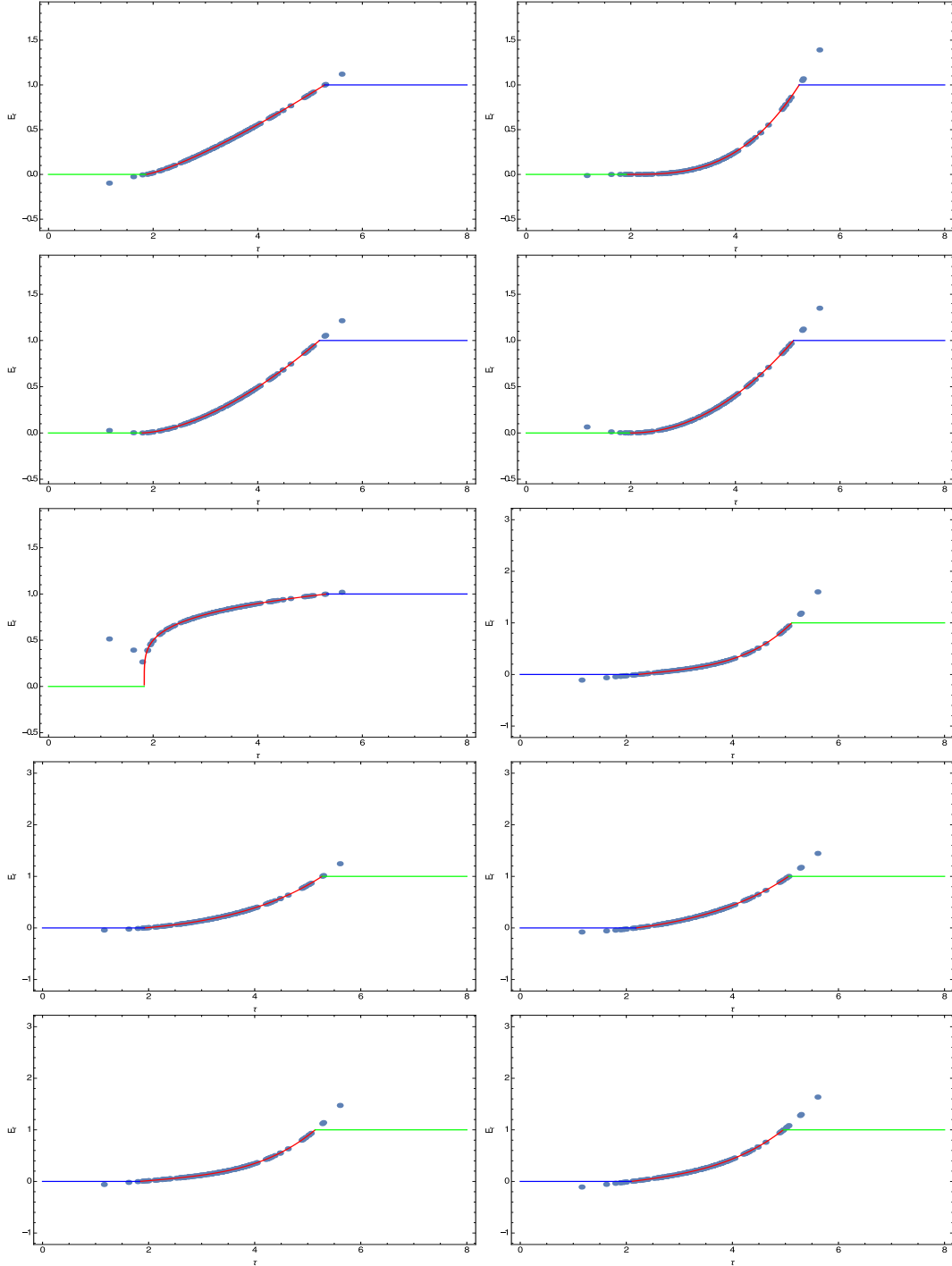


Fig. 6.— The first 5 panels represent examples of the efficiency function for the linear case versus the times, τ of the GRBs in our data sample, while the last 5 panels the efficiency functions for the fourth order polynomial. The linear functions as well the polynomial ones are computed according to Eq. 18, and Eq. 19.

τ_L , see Fig. 6.

4. REDSHIFT EVOLUTION ON THE NORMALIZATION AND SLOPE PARAMETERS

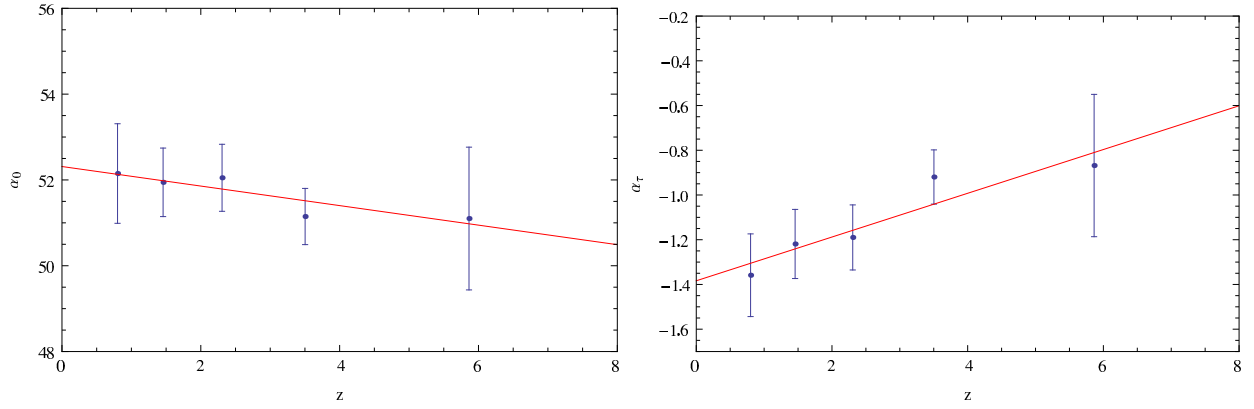


Fig. 7.— α_τ and normalization α_0 using a linear function $\alpha_0 = -0.22x + 52.31$ (left panel) and $\alpha_\tau = 0.10x - 1.38$ (right panel).

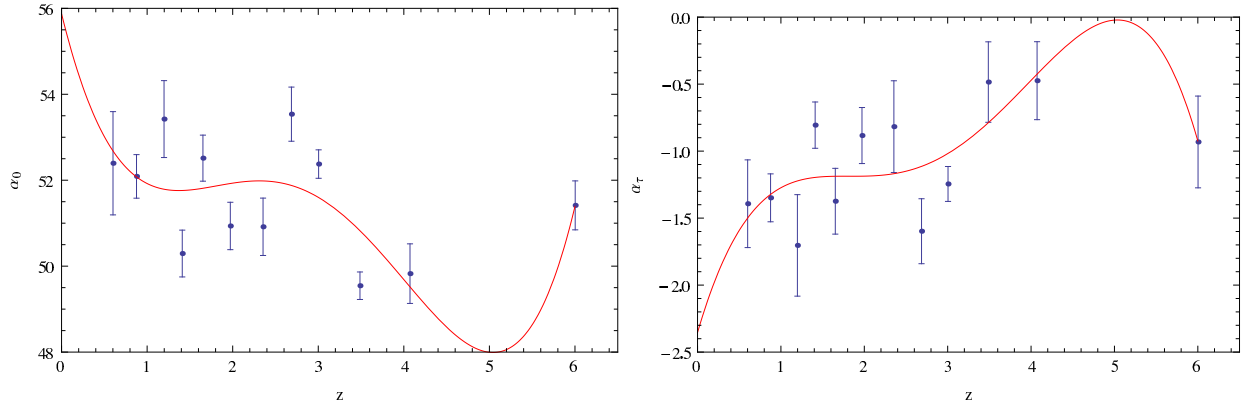


Fig. 8.— α_τ and normalization α_0 using a polynomial function $\alpha_0 = 55.87 - 8.13x + 5.53x^2 - 1.48x^3 + 0.13x^4$ (left panel) and $\alpha_\tau = -2.35 + 2.13x - 1.39x^2 + 0.37x^3 - 0.03x^4$ (right panel).

As we have already mentioned in the previous paragraph the polynomial and the linear model for the $\epsilon(\lambda)$ are unknown, then assumptions need to be made. We chose these forms, because both normalization and slope of the LT correlation depend on the redshift either with a polynomial or with a simple power law. Therefore, these choices for the selection functions take into account of this redshift dependence. Namely, we consider a model redshift

Id	λ_L	λ_U	\mathcal{E}_λ	$P_{GRB,rate}$
PL1	44.34	50.86	1.25	$\leq 10^{-4}$
PL2	43.64	49.87	2.99	0.003
PL3	43.77	50.74	1.65	0.53
PL4	44.77	49.59	2.04	0.001
PL5	44.14	50.83	0.23	0.54

Table 1: Efficiency function parameters for the power-law \mathcal{E}_λ and no cut on τ i.e. $\mathcal{E}_\tau = 1$. $P_{GRB,rate}$ is the goodness of fit between our data and the observed GRBs rate density, thus how the data well fit the observed GRBs density rate. To compute the probability we compute the χ^2 test that performs a statistical hypothesis test in which the sampling distribution of the test statistic is a χ^2 distribution when the null hypothesis is true, in order to determine whether there is a significant difference between the expected frequencies and the observed frequencies.

Id	λ_L	λ_U	\mathcal{E}_1	\mathcal{E}_2	\mathcal{E}_3	\mathcal{E}_4	$P_{GRB,rate}$
PoL1	44.90	49.14	0.46	0.01	0.24	0.80	0.54
PoL2	41.10	50.23	0.60	0.95	0.05	0.53	$\leq 10^{-4}$
PoL3	43.57	49.09	0.71	0.79	0.07	0.34	0.019
PoL4	44.37	49.52	0.51	0.03	0.46	0.78	0.15
PoL5	43.03	50.06	0.79	0.36	0.63	0.40	0.001

Table 2: Same as table 1 but for the polynomial functions. $P_{GRB,rate}$ is the goodness of fit between our data and the observed GRB rate density.

dependence because of the corresponding dependence of both luminosity and time. This has been already shown in Dainotti et al. (2013a) and currently in the middle panel of Fig. 3 for the updated data sample. To study the behavior of the redshift evolution we plot the slope and the normalization values versus the redshift. These are obtained from the average values for the data set divided into 5 bins, see figure 7 and into 12 bins, see figure 8. As we can see from both figures 7 and 8 the normalization parameter α_0 decreases as the redshift increases, while the slope parameter α_τ shows the opposite trend. Goodness of the fits is given by the probability $P = 0.79$ for the data set divided in 5 bins and $P = 0.87$ for the one divided into 12 bins for the linear case, while for the polynomial model $P = 0.99$ and $P = 0.94$ for the data set divided in 5 and 12 bins respectively. These results show that both polynomial and linear fit are possible.

5. IMPACT OF SELECTION EFFECTS

The simulated samples generated as described above are input to the same Bayesian fitting procedure we use with real data. For each input $(\alpha_\tau, \alpha_\zeta, \alpha_0, \sigma_{int})$ parameters, we simulate ~ 50 GRBs sample setting $\mathcal{N}_{sim} = 200$, while the number of observed GRBs depend on the efficiency function used. We fit these samples assuming no redshift evolution in Eq. 1, i.e. forcing $\alpha_\zeta = 0$ in the fit so that, for each simulated sample, the fitting procedure returns both the best fit and the median and 68% confidence range of the parameters $(\alpha_\tau, \alpha_0, \sigma_{int})$. In order to investigate whether the selection effects impact the recovery of the input scaling laws, we fit linear relations of the form:

$$x_f = ax_{inp} + b \tag{20}$$

where x_{inp} is the input value and x_f can be either the best fit (denoted as x_{bf}) or the median x_{fit} value. When fitting the above linear relation, we use the χ^2 minimization for x_{bf} , while a weighted fit is performed for x_{fit} with weights $\omega_i = 1/\sigma_i^2$ where σ_i is the symmetrized 1σ error. Note that the label i here runs over the simulations performed for each given efficiency function.

5.1. No redshift evolution

Here, we consider input models with $\alpha_\zeta = 0$, i.e. no redshift evolution of the scaling law (1). It is worth noting that such an assumption is actually well motivated since it has been demonstrated in Dainotti et al. (2013a) that luminosity is almost not affected by redshift

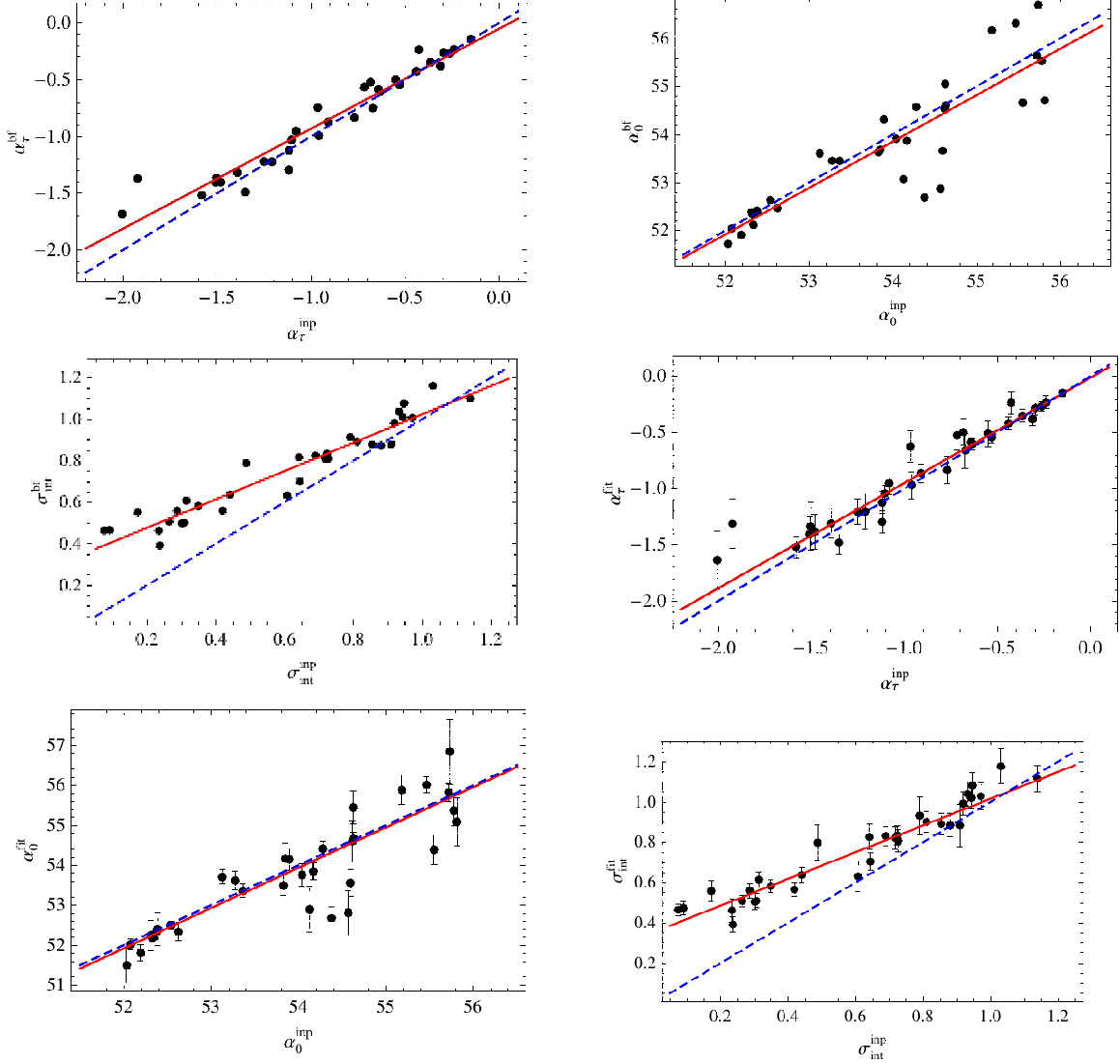


Fig. 9.— Fitted vs input (α_τ , α_0 , σ_{int}) parameters obtained with the power law function. The first three panels refer to the best fit values, while the other three show the median values with the 1σ error bars. Solid red line is the best fit line while blue dashed is the no bias line when $x_{inp} = x_f$.

evolution, while time becomes to undergo redshift evolution for high redshift only. From our point of view, however, this case allows us to directly quantify the impact of the efficiency functions on the recovery of the scaling correlation parameters since any deviation will only be due to the selection effects and not to any attempt of compensating the missed evolution with z .

5.1.1. No selection on τ ($\mathcal{E}_\tau = 1$)

We start by considering the idealized case of no selection of τ , i.e., we force $\mathcal{E}_\tau = 1$, and set the \mathcal{E}_λ parameters as listed in Tables 1 and 2 for the power-law and polynomial expressions, respectively. As an example, figure 9 shows the results for the efficiency function, while Table 3 summarizes the (a, b) coefficients of the linear fit between the input and recovered quantities. The closer is a to 1, the less is the parameter biased, while $b \neq 0$ should not be taken as evidence for bias. This result is in perfect agreement with the intrinsic correlation slope, which is $-1.07^{+0.09}_{-0.14}$ (Dainotti et al. 2013b), when we consider as the best choice for the selection functions the ones that returns values of a closer to 1. If Equation 20 is fulfilled, we can estimate the relative bias as:

$$\frac{\Delta x}{x} = \frac{x_{inp} - x_f}{x_{inp}} = 1 - a - \frac{b}{x_{inp}}, \quad (21)$$

so that we can accept $b \neq 0$ if x_{inp} is much larger than b . This is indeed the case for $x_{inp} = \alpha_0$ which takes typical values (~ 50) much larger than the b ones in Table 3. From the proximity between solid and dashed lines, which represent respectively the best fit line and the no bias line when $x_{inp} = x_f$, in the corresponding panels of Fig. 9, we see that, for the power-law efficiency function (and no cut on τ), both the slope and the zero point of the scaling relation are correctly recovered. The reason why is that the relative bias is

Id	$(a, b)_{bf}^\tau$	$(a, b)_{fit}^\tau$	$(a, b)_{bf}^{\alpha_0}$	$(a, b)_{fit}^{\alpha_0}$	$(a, b)_{bf}^\sigma$	$(a, b)_{fit}^\sigma$	$\frac{\Delta x}{x}$
PL1	(0.953,0.010)	(0.959,0.013)	(0.928,3.688)	(1.000,-0.073)	(0.593,0.354)	(0.616,0.355)	0.004
PL2	(0.914,-0.008)	(0.873,-0.024)	(1.013,-0.836)	(0.989,0.292)	(0.689,0.299)	(0.643,0.341)	0.002
PL3	(0.880,-0.052)	(0.937,-0.013)	(0.965,1.729)	(1.008,-0.513)	(0.683,0.340)	(0.664,0.352)	0.003
PL4	(0.946,0.024)	(0.964,0.024)	(0.995,-0.076)	(1.086,-4.905)	(0.614,0.364)	(0.585,0.380)	0.006
PL5	(0.916,-0.030)	(0.962,0.004)	(1.033,-2.067)	(0.828,9.095)	(0.716,0.333)	(0.679,0.356)	0.005

Table 3: Slope a and zero point b of the fitted vs input parameters for both the best fit and median values (labeled with subscripts bf and fit , respectively). The upperscript denotes the parameter fitted with (τ, α_0, σ) referring to $(\alpha_\tau, \alpha_0, \sigma_{int})$, respectively. $\frac{\Delta x}{x}$ is the bias for each efficiency function considered.

negligible small notwithstanding the values of the parameters setting \mathcal{E}_λ . This is particularly true if one relies on the median values as estimate since they are typically consistent with the no bias line within less than 2σ .

The above results have been obtained considering a power-law \mathcal{E}_λ so that it is worth investigating whether they critically depend on this assumption. We have therefore repeated the analysis for the polynomial \mathcal{E}_λ models in Table 2 obtaining the results in Table 4. A comparison with the values in Table 4 shows that the (a, b) coefficients are similar so that one could preliminarily conclude that the shape of the efficiency function does not play a major role in the determination of the bias. Actually, although the functional expressions are different, both the power-law and the polynomial selection functions are qualitatively similar with \mathcal{E}_λ increasing with λ over a comparable range. Although such a behaviour is likely common to any reasonable \mathcal{E}_λ , we can not exclude a priori that non monotonic selection functions do actually exist. What would the results be in such a case is not clear so that we prefer to be cautious and conclude that the bias is roughly the same whichever monotonic $\mathcal{E}_\lambda(\lambda)$ function is used, but not for all the possible \mathcal{E}_λ functions. For non-monotonic shape of selection function, see Stern et al. (2001), in which an assumed detection efficiency function, defined as the ratio of the number of detected test bursts to the number of test bursts applied to the data versus the expected peak count rate, is given by:

$$E(c_e) = 0.70 \times [1 - \exp[-(\frac{c_e}{c_{e,0}})^2]]^\nu, \tag{22}$$

where $c_{e,0} = 0.097$ counts $s^{-1} cm^{-2}$ and $\nu = 2.34$ are two constants. However, quoting from Stern et al. (2001), the best possible efficiency quality has still not yet been achieved because in fact the detection efficiency depends on the peak count rate rather than on the time-integrated signal.

Id	$(a, b)_{bf}^\tau$	$(a, b)_{fit}^\tau$	$(a, b)_{bf}^{\alpha_0}$	$(a, b)_{fit}^{\alpha_0}$	$(a, b)_{bf}^\sigma$	$(a, b)_{fit}^\sigma$	$\frac{\Delta_x}{x}$
PoL1	(0.950,0.020)	(0.928,0.011)	(1.099,-5.545)	(1.178,-9.935)	(0.647,0.350)	(0.673,0.349)	0.004
PoL2	(1.095,0.128)	(1.075,0.105)	(1.030,-1.662)	(1.023,-1.278)	(0.681,0.337)	(0.625,0.372)	0.0008
PoL3	(0.984,0.063)	(0.936,0.015)	(0.711,15.258)	(0.988,0.376)	(0.741,0.289)	(0.685,0.336)	0.007
PoL4	(0.870,-0.025)	(0.969,0.052)	(0.730,14.103)	(0.734,13.872)	(0.630,0.351)	(0.582,0.381)	0.009
PoL5	(1.004,0.069)	(0.972,0.030)	(0.963,11.772)	(1.002,-0.374)	(0.581,0.384)	(0.549,0.402)	0.18

Table 4: Same as Table 3 but for the polynomial \mathcal{E}_λ model.

5.1.2. Selection cuts on both τ and λ

We now consider the case where the total selection function may be factorized as $\mathcal{E}(\tau, \lambda) = \mathcal{E}_\tau(\tau)\mathcal{E}_\lambda(\lambda)$ with both $\mathcal{E}_x(x)$ functions being given by power-law or fourth order polynomial expressions. We consider 10 different arbitrary choices for both cases. Note that we have to increase \mathcal{N}_{sim} to 300 in order to have $\mathcal{N}_{obs} = 80 - 100$ as for the models discussed in the previous subsection.

Table 5 gives the (a,b) coefficients for the different models considered. A comparison with Table 3 shows that, on average, the bias on the parameters is roughly the same with the median values giving smaller deviations and significant bias on σ_{int} only. A more detailed analysis, however, shows that, while, in the $\mathcal{E}_\tau = 1$ case, biases larger than 5% are of the order of 10%. Namely, from Table 3 and 4 we show that the relative biases, $\frac{\Delta_x}{x}$, both in the linear and the polynomial case, give very small values from 0.2% to 0.9%, with the only exception of 1 polynomial function, in which the bias is 18%, thus giving $P = 10\%$ of having larger bias than 5%. If we consider selection cuts on both τ and λ we notice in Table 5 that number of bias whose value is greater than 5% are 4, thus increasing their probability to occur ($P \sim 40\%$). This can be qualitatively explained noting that a cut on λ only removes the points in the luminosity axis thus possibly shifting the best fit relation, but not changing the slope. On the contrary, removing points also along the horizontal τ axis can change the slope α_τ too and hence also affects (α_0, σ_{int}) because of the correlation among these parameters and α_τ . Similar results are obtained when both \mathcal{E}_x functions are modeled with fourth order polynomials so that we will not discuss this case here. We stress that when $\frac{\Delta_x}{x}$ are larger than 6%, than the slope of the correlation is farther from -1.0 compared to cases in which $\frac{\Delta_x}{x} \leq 0.06$. In fact, in the first case the slopes values range from 0.86 to 0.91, see the functions *PLTa4* and *PLTa6* in Table 5. These values are not compatible in 1σ with the claimed intrinsic slope of the correlation, $-1.07^{+0.09}_{-0.14}$. If we consider, instead, the lowest $\frac{\Delta_x}{x}$, then we obtain ranges of $a = (0.94, 0.99)$ thus showing full compatibility in 1σ with the intrinsic slope. In this way we have quantitatively confirmed the existence of the $L_X - T_a^*$ correlation with the same intrinsic slope as in Dainotti et al. (2013a) if appropriate selection functions are chosen.

6. Conclusions

Here we built a general method to evaluate selection effects for GRB correlations not knowing a priori the efficiency function of the detector used. We have tested this method on the LT correlation. We chose a set of GRBs and assuming Gaussian distributions for the variables involved, for luminosity and time, and also a particular shape for the GRBs

rate density. We simulated a mock sample of data in order to consider the selection effects of the detectors. As we can see in paragraph 3 assuming the correct observed GRBs rate density shape was not an easy task. In fact, we explored different methods (Li 2008; Robertson and Ellis 2012; Kistler et al. 2013; Hopkins and Beacom 2006) that use several SFR shapes to understand which one best matches the afterglow plateau data distribution including the selection functions, see Fig. 4. The most reliable fits for the GRB plateau data is the SFR used by Li (2008), while the best efficiency functions for $\epsilon(\lambda)$ that match the GRB density rate can be both two polynomial and two linear, see Fig. 4. Table 1 and 2 show the probability that the density rate fits the afterglow plateau GRB rate assuming those efficiency functions. However, we assumed there could be selection effects both for luminosity and time. In particular, the bias is roughly the same whichever monotonic efficiency function for the luminosity detection \mathcal{E}_λ is taken. From Table 3 and 4 we show that the relative biases, $\frac{\Delta_x}{x}$, both in the linear and the polynomial case, give very small values from 0.2% to 0.9%, with the only exception of 1 polynomial function, in which the bias is 18%, thus giving $P = 10\%$ of having larger bias than 5%. If we consider selection cuts on both τ and λ we notice in Table 5 that number of bias whose value is greater than 5% are 4, thus increasing the probability of having such biases ($P \sim 40\%$). In addition, we studied selection effects in the LT correlation assuming also a combination of the luminosity and time detection efficiency functions. Different values for the parameters of the efficiency functions in the detectors are taken into account as described in the paragraph 5. This gives distinct fit values that inserted in Equation 20 allow to study the scattering of the correlation and its selection effects. We have quantitatively confirmed the existence of the $L_X - T_a^*$ correlation with the same intrinsic slope as in Dainotti et al. (2013a) if appropriate selection functions are chosen. In particular, when $\frac{\Delta_x}{x}$ are larger than 6%, than the slope of the correlation is farther from -1.0 compared to cases in which $\frac{\Delta_x}{x} \leq 0.06$. The lowest $\frac{\Delta_x}{x}$ leads to ranges of $a = (0.94, 0.99)$ thus showing full compatibility in 1σ with the intrinsic slope. Finally, the fact that the correlation is not generated by the biases themselves is a significant and further step towards considering a set of GRBs as standard candles and their possible and useful application as a cosmological tool.

7. Acknowledgements

This work made use of data supplied by the UK Swift Science Data Centre at the University of Leicester. We are particularly grateful to Cardone, V.F. for the initial contribution to this work. M.G.D. and S.N. are grateful to the iTHES Group discussions at Riken. M.D is grateful to the support from the JSPS Foundation, (No. 25.03786). N. S. is grateful to JSPS (No.24.02022, No.25.03018, No.25610056, No.26287056) & MEXT(No.26105521), R.

D.V. is grateful to 2012/04/A/ST9/00083.

REFERENCES

- L. Amati, F. Frontera, and C. Guidorzi. Extremely energetic Fermi gamma-ray bursts obey spectral energy correlations. *A&A*, 508:173–180, December 2009. doi: 10.1051/0004-6361/200912788.
- D. L. Band. Postlaunch Analysis of Swift’s Gamma-Ray Burst Detection Sensitivity. *ApJ*, 644:378–384, June 2006. doi: 10.1086/503326.
- M. G. Bernardini, R. Margutti, J. Mao, E. Zaninoni, and G. Chincarini. The X-ray light curve of gamma-ray bursts: clues to the central engine. *A&A*, 539:A3, March 2012a. doi: 10.1051/0004-6361/201117895.
- M. G. Bernardini, R. Margutti, E. Zaninoni, and G. Chincarini. A universal scaling for short and long gamma-ray bursts: $E_{X,iso} - E_{,iso} - E_{pk}$. *MNRAS*, 425:1199–1204, September 2012b. doi: 10.1111/j.1365-2966.2012.21487.x.
- J. S. Bloom. Is the Redshift Clustering of Long-Duration Gamma-Ray Bursts Significant? *AJ*, 125:2865–2875, June 2003. doi: 10.1086/374945.
- N. R. Butler, J. S. Bloom, and D. Poznanski. The Cosmic Rate, Luminosity Function, and Intrinsic Correlations of Long Gamma-Ray Bursts. *ApJ*, 711:495–516, March 2010. doi: 10.1088/0004-637X/711/1/495.
- J. I. Cabrera, C. Firmani, V. Avila-Reese, G. Ghirlanda, G. Ghisellini, and L. Nava. Spectral analysis of Swift long gamma-ray bursts with known redshift. *MNRAS*, 382:342–355, November 2007. doi: 10.1111/j.1365-2966.2007.12374.x.
- J. K. Cannizzo and N. Gehrels. A New Paradigm for Gamma-ray Bursts: Long-term Accretion Rate Modulation by an External Accretion Disk. *ApJ*, 700:1047–1058, August 2009. doi: 10.1088/0004-637X/700/2/1047.
- J. K. Cannizzo, E. Troja, and N. Gehrels. Fall-back Disks in Long and Short Gamma-Ray Bursts. *ApJ*, 734:35, June 2011. doi: 10.1088/0004-637X/734/1/35.
- V. F. Cardone, S. Capozziello, and M. G. Dainotti. An updated gamma-ray bursts Hubble diagram. *MNRAS*, 400:775–790, December 2009. doi: 10.1111/j.1365-2966.2009.15456.x.

- V. F. Cardone, M. G. Dainotti, S. Capozziello, and R. Willingale. Constraining cosmological parameters by gamma-ray burst X-ray afterglow light curves. *MNRAS*, 408:1181–1186, October 2010. doi: 10.1111/j.1365-2966.2010.17197.x.
- D. Coward. Open issues with the gamma-ray burst redshift distribution. *New A Rev.*, 51: 539–546, September 2007. doi: 10.1016/j.newar.2007.03.003.
- A. Cucchiara, A. J. Levan, D. B. Fox, N. R. Tanvir, T. N. Ukwatta, E. Berger, T. Krühler, A. Küpcü Yoldaş, X. F. Wu, K. Toma, J. Greiner, F. E. Olivares, A. Rowlinson, L. Amati, T. Sakamoto, K. Roth, A. Stephens, A. Fritz, J. P. U. Fynbo, J. Hjorth, D. Malesani, P. Jakobsson, K. Wiersema, P. T. O’Brien, A. M. Soderberg, R. J. Foley, A. S. Fruchter, J. Rhoads, R. E. Rutledge, B. P. Schmidt, M. A. Dopita, P. Podsiadlowski, R. Willingale, C. Wolf, S. R. Kulkarni, and P. D’Avanzo. A Photometric Redshift of $z \sim 9.4$ for GRB 090429B. *ApJ*, 736:7, July 2011. doi: 10.1088/0004-637X/736/1/7.
- G. D’Agostini. Fits, and especially linear fits, with errors on both axes, extra variance of the data points and other complications. *ArXiv Physics e-prints*, November 2005.
- F. Daigne and R. Mochkovitch. The low-luminosity tail of the GRB distribution: the case of GRB 980425. *A&A*, 465:1–8, April 2007. doi: 10.1051/0004-6361:20066080.
- M. G. Dainotti, V. F. Cardone, and S. Capozziello. A time-luminosity correlation for γ -ray bursts in the X-rays. *MNRAS*, 391:L79–L83, November 2008. doi: 10.1111/j.1745-3933.2008.00560.x.
- M. G. Dainotti, R. Willingale, S. Capozziello, V. Fabrizio Cardone, and M. Ostrowski. Discovery of a Tight Correlation for Gamma-ray Burst Afterglows with ”Canonical” Light Curves. *ApJ*, 722:L215–L219, October 2010. doi: 10.1088/2041-8205/722/2/L215.
- M. G. Dainotti, V. Fabrizio Cardone, S. Capozziello, M. Ostrowski, and R. Willingale. Study of Possible Systematics in the L^*_X - T^*_a Correlation of Gamma-ray Bursts. *ApJ*, 730: 135, April 2011a. doi: 10.1088/0004-637X/730/2/135.
- M. G. Dainotti, M. Ostrowski, and R. Willingale. Towards a standard gamma-ray burst: tight correlations between the prompt and the afterglow plateau phase emission. *MNRAS*, 418:2202–2206, December 2011b. doi: 10.1111/j.1365-2966.2011.19433.x.
- M. G. Dainotti, V. F. Cardone, E. Piedipalumbo, and S. Capozziello. Slope evolution of GRB correlations and cosmology. *MNRAS*, 436:82–88, November 2013a. doi: 10.1093/mnras/stt1516.

- M. G. Dainotti, V. Petrosian, J. Singal, and M. Ostrowski. Determination of the Intrinsic Luminosity Time Correlation in the X-Ray Afterglows of Gamma-Ray Bursts. *ApJ*, 774:157, September 2013b. doi: 10.1088/0004-637X/774/2/157.
- S. Dall’Osso, G. Stratta, D. Guetta, S. Covino, G. De Cesare, and L. Stella. Gamma-ray bursts afterglows with energy injection from a spinning down neutron star. *A&A*, 526:A121, February 2011. doi: 10.1051/0004-6361/201014168.
- B. Efron and V. Petrosian. A simple test of independence for truncated data with applications to redshift surveys. *ApJ*, 399:345–352, November 1992. doi: 10.1086/171931.
- E. E. Fenimore and E. Ramirez-Ruiz. Redshifts For 220 BATSE Gamma-Ray Bursts Determined by Variability and the Cosmological Consequences. *ArXiv Astrophysics e-prints*, April 2000.
- F. Fiore, D. Guetta, S. Piranomonte, V. D’Elia, and L. A. Antonelli. Selection effects shaping the gamma ray burst redshift distributions. *A&A*, 470:515–522, August 2007. doi: 10.1051/0004-6361:20077157.
- G. Ghirlanda, G. Ghisellini, and D. Lazzati. The Collimation-corrected Gamma-Ray Burst Energies Correlate with the Peak Energy of Their νF_{ν} Spectrum. *ApJ*, 616:331–338, November 2004. doi: 10.1086/424913.
- G. Ghirlanda, G. Ghisellini, and C. Firmani. Gamma-ray bursts as standard candles to constrain the cosmological parameters. *New Journal of Physics*, 8:123, July 2006. doi: 10.1088/1367-2630/8/7/123.
- G. Ghisellini, M. Nardini, G. Ghirlanda, and A. Celotti. A unifying view of gamma-ray burst afterglows. *MNRAS*, 393:253–271, February 2009. doi: 10.1111/j.1365-2966.2008.14214.x.
- D. Guetta and M. Della Valle. On the Rates of Gamma-Ray Bursts and Type Ib/c Supernovae. *ApJ*, 657:L73–L76, March 2007. doi: 10.1086/511417.
- R. Hascoët, F. Daigne, and R. Mochkovitch. The prompt-early afterglow connection in gamma-ray bursts: implications for the early afterglow physics. *MNRAS*, 442:20–27, July 2014. doi: 10.1093/mnras/stu750.
- A. M. Hopkins and J. F. Beacom. On the Normalization of the Cosmic Star Formation History. *ApJ*, 651:142–154, November 2006. doi: 10.1086/506610.

- L. Izzo, G. B. Pisani, M. Muccino, J. A. Rueda, Y. Wang, C. L. Bianco, A. V. Penacchioni, and R. Ruffini. A common behavior in the late X-ray afterglow of energetic GRB-SN systems. In A. J. Castro-Tirado, J. Gorosabel, and I. H. Park, editors, *EAS Publications Series*, volume 61 of *EAS Publications Series*, pages 595–597, July 2013. doi: 10.1051/eas/1361095.
- P. Jakobsson, A. Levan, J. P. U. Fynbo, R. Priddey, J. Hjorth, N. Tanvir, D. Watson, B. L. Jensen, J. Sollerman, P. Natarajan, J. Gorosabel, J. M. Castro Cerón, K. Pedersen, T. Pursimo, A. S. Árnadóttir, A. J. Castro-Tirado, C. J. Davis, H. J. Deeg, D. A. Fiuza, S. Mikolaitis, and S. G. Sousa. A mean redshift of 2.8 for Swift gamma-ray bursts. *A&A*, 447:897–903, March 2006. doi: 10.1051/0004-6361:20054287.
- M. D. Kistler, H. Yüksel, J. F. Beacom, and K. Z. Stanek. An Unexpectedly Swift Rise in the Gamma-Ray Burst Rate. *ApJ*, 673:L119–L122, February 2008. doi: 10.1086/527671.
- M. D. Kistler, H. Yuksel, and A. M. Hopkins. The Cosmic Star Formation Rate from the Faintest Galaxies in the Unobservable Universe. *ArXiv e-prints*, May 2013.
- D. Kocevski and V. Petrosian. On the Lack of Time Dilation Signatures in Gamma-Ray Burst Light Curves. *ApJ*, 765:116, March 2013. doi: 10.1088/0004-637X/765/2/116.
- T. Le and C. D. Dermer. On the Redshift Distribution of Gamma-Ray Bursts in the Swift Era. *ApJ*, 661:394–415, May 2007. doi: 10.1086/513460.
- K. Leventis, R. A. M. J. Wijers, and A. J. van der Horst. The plateau phase of gamma-ray burst afterglows in the thick-shell scenario. *MNRAS*, 437:2448–2460, January 2014. doi: 10.1093/mnras/stt2055.
- L.-X. Li. The X-ray transient 080109 in NGC 2770: an X-ray flash associated with a normal core-collapse supernova. *MNRAS*, 388:603–610, August 2008. doi: 10.1111/j.1365-2966.2008.13461.x.
- N. M. Lloyd and V. Petrosian. Distribution of Spectral Characteristics and the Cosmological Evolution of Gamma-Ray Bursts. *ApJ*, 511:550–561, February 1999. doi: 10.1086/306719.
- J. Mao. A Theoretical Investigation of Gamma-ray Burst Host Galaxies. *ApJ*, 717:140–146, July 2010. doi: 10.1088/0004-637X/717/1/140.
- S. Mao and H. J. Mo. The nature of the host galaxies for gamma-ray bursts. *A&A*, 339:L1–L4, November 1998.

- P. Natarajan, B. Albanna, J. Hjorth, E. Ramirez-Ruiz, N. Tanvir, and R. Wijers. The redshift distribution of gamma-ray bursts revisited. *MNRAS*, 364:L8–L12, November 2005. doi: 10.1111/j.1745-3933.2005.00094.x.
- R. S. Nemmen, M. Georganopoulos, S. Guiriec, E. T. Meyer, N. Gehrels, and R. M. Sambruna. A Universal Scaling for the Energetics of Relativistic Jets from Black Hole Systems. *Science*, 338:1445–, December 2012. doi: 10.1126/science.1227416.
- J. P. Norris, G. F. Marani, and J. T. Bonnell. Connection between Energy-dependent Lags and Peak Luminosity in Gamma-Ray Bursts. *ApJ*, 534:248–257, May 2000. doi: 10.1086/308725.
- P. T. O’Brien, R. Willingale, J. Osborne, M. R. Goad, K. L. Page, S. Vaughan, E. Rol, A. Beardmore, O. Godet, C. P. Hurkett, A. Wells, B. Zhang, S. Kobayashi, D. N. Burrows, J. A. Nousek, J. A. Kennea, A. Falcone, D. Grupe, N. Gehrels, S. Barthelmy, J. Cannizzo, J. Cummings, J. E. Hill, H. Krimm, G. Chincarini, G. Tagliaferri, S. Campana, A. Moretti, P. Giommi, M. Perri, V. Mangano, and V. LaParola. The Early X-Ray Emission from GRBs. *ApJ*, 647:1213–1237, August 2006. doi: 10.1086/505457.
- V. Petrosian. New Statistical Methods for Analysis of Large Surveys: Distributions and Correlations. In R. F. Green, E. Y. Khachikian, and D. B. Sanders, editors, *IAU Colloq. 184: AGN Surveys*, volume 284 of *Astronomical Society of the Pacific Conference Series*, page 389, 2002.
- V. Petrosian and N. M. Lloyd. The νF_{ν} Peak Energy of Gamma Ray Bursts, and its Correlation with Fluence and Peak Flux. In *American Astronomical Society Meeting Abstracts*, volume 30 of *Bulletin of the American Astronomical Society*, page 1380, December 1998.
- V. Petrosian, N. Lloyd, and A. Lee. Cosmological Signatures in Temporal and Spectral Characteristics of Gamma-Ray Bursts. In J. Poutanen and R. Svensson, editors, *Gamma-Ray Bursts: The First Three Minutes*, volume 190 of *Astronomical Society of the Pacific Conference Series*, page 235, 1999.
- C. Porciani and P. Madau. On the Association of Gamma-Ray Bursts with Massive Stars: Implications for Number Counts and Lensing Statistics. *ApJ*, 548:522–531, February 2001. doi: 10.1086/319027.
- S. Postnikov, M. G. Dainotti, X. Hernandez, and S. Capozziello. Nonparametric Study of the Evolution of the Cosmological Equation of State with SNeIa, BAO, and High-redshift GRBs. *ApJ*, 783:126, March 2014. doi: 10.1088/0004-637X/783/2/126.

- S. Qi and T. Lu. Toward Tight Gamma-Ray Burst Luminosity Relations. *ApJ*, 749:99, April 2012. doi: 10.1088/0004-637X/749/2/99.
- B. E. Robertson and R. S. Ellis. Connecting the Gamma Ray Burst Rate and the Cosmic Star Formation History: Implications for Reionization and Galaxy Evolution. *ApJ*, 744:95, January 2012. doi: 10.1088/0004-637X/744/2/95.
- A. Rowlinson, P. T. O’Brien, N. R. Tanvir, B. Zhang, P. A. Evans, N. Lyons, A. J. Levan, R. Willingale, K. L. Page, O. Onal, D. N. Burrows, A. P. Beardmore, T. N. Ukwatta, E. Berger, J. Hjorth, A. S. Fruchter, R. L. Tunnicliffe, D. B. Fox, and A. Cucchiara. The unusual X-ray emission of the short Swift GRB 090515: evidence for the formation of a magnetar? *MNRAS*, 409:531–540, December 2010. doi: 10.1111/j.1365-2966.2010.17354.x.
- A. Rowlinson, P. T. O’Brien, B. D. Metzger, N. R. Tanvir, and A. J. Levan. Signatures of magnetar central engines in short GRB light curves. *MNRAS*, 430:1061–1087, April 2013. doi: 10.1093/mnras/sts683.
- A. Rowlinson, B. P. Gompertz, M. Dainotti, P. T. O’Brien, R. A. M. J. Wijers, and A. J. van der Horst. Constraining properties of GRB magnetar central engines using the observed plateau luminosity and duration correlation. *MNRAS*, 443:1779–1787, September 2014. doi: 10.1093/mnras/stu1277.
- T. Sakamoto, J. E. Hill, R. Yamazaki, L. Angelini, H. A. Krimm, G. Sato, S. Swindell, K. Takami, and J. P. Osborne. Evidence of Exponential Decay Emission in the Swift Gamma-Ray Bursts. *ApJ*, 669:1115–1129, November 2007. doi: 10.1086/521640.
- B. E. Schaefer. Explaining the Gamma-Ray Burst E_{peak} Distribution. *ApJ*, 583:L71–L74, February 2003. doi: 10.1086/368106.
- A. Shahmoradi and R. Nemiroff. How Real Detector Thresholds Create False Standard Candles. In C. Meegan, C. Kouveliotou, and N. Gehrels, editors, *American Institute of Physics Conference Series*, volume 1133 of *American Institute of Physics Conference Series*, pages 425–427, May 2009. doi: 10.1063/1.3155940.
- B. E. Stern, Y. Tikhomirova, D. Kompaneets, R. Svensson, and J. Poutanen. An Off-Line Scan of the BATSE Daily Records and a Large Uniform Sample of Gamma-Ray Bursts. *ApJ*, 563:80–94, December 2001. doi: 10.1086/322295.
- J. Sultana, D. Kazanas, and K. Fukumura. Luminosity Correlations for Gamma-Ray Bursts and Implications for Their Prompt and Afterglow Emission Mechanisms. *ApJ*, 758:32, October 2012. doi: 10.1088/0004-637X/758/1/32.

- T. Totani. Cosmological Gamma-Ray Bursts and Evolution of Galaxies. *ApJ*, 486:L71–L74, September 1997. doi: 10.1086/310853.
- H. van Eerten. Self-similar relativistic blast waves with energy injection. *MNRAS*, 442: 3495–3510, August 2014a. doi: 10.1093/mnras/stu1025.
- H. J. van Eerten. Gamma-ray burst afterglow plateau break time-luminosity correlations favour thick shell models over thin shell models. *MNRAS*, 445:2414–2423, December 2014b. doi: 10.1093/mnras/stu1921.
- R. A. M. J. Wijers, J. S. Bloom, J. S. Bagla, and P. Natarajan. Gamma-ray bursts from stellar remnants - Probing the universe at high redshift. *MNRAS*, 294:L13–L17, February 1998. doi: 10.1046/j.1365-8711.1998.01328.x.
- R. Willingale, P. T. O’Brien, J. P. Osborne, O. Godet, K. L. Page, M. R. Goad, D. N. Burrows, B. Zhang, E. Rol, N. Gehrels, and G. Chincarini. Testing the Standard Fireball Model of Gamma-Ray Bursts Using Late X-Ray Afterglows Measured by Swift. *ApJ*, 662:1093–1110, June 2007. doi: 10.1086/517989.
- R. Yamazaki. Prior Emission Model for X-ray Plateau Phase of Gamma-Ray Burst Afterglows. *ApJ*, 690:L118–L121, January 2009. doi: 10.1088/0004-637X/690/2/L118.
- D. Yonetoku, T. Murakami, T. Nakamura, R. Yamazaki, A. K. Inoue, and K. Ioka. Gamma-Ray Burst Formation Rate Inferred from the Spectral Peak Energy-Peak Luminosity Relation. *ApJ*, 609:935–951, July 2004. doi: 10.1086/421285.
- B. Yu, S. Qi, and T. Lu. Gamma-ray Burst Luminosity Relations: Two-Dimensional Versus Three-Dimensional Correlations. *ApJ*, 705:L15–L19, November 2009. doi: 10.1088/0004-637X/705/1/L15.
- H. Yüksel and M. D. Kistler. Enhanced cosmological GRB rates and implications for cosmogenic neutrinos. *Phys. Rev. D*, 75(8):083004, April 2007. doi: 10.1103/PhysRevD.75.083004.

Id	$(a, b)_{bf}^{\tau}$	$(a, b)_{fit}^{\tau}$	$(a, b)_{bf}^{\alpha_0}$	$(a, b)_{fit}^{\alpha_0}$	$(a, b)_{bf}^{\sigma}$	$(a, b)_{fit}^{\sigma}$	$\frac{\Delta_x}{x}$
PLTa1	(0.842,-0.080)	(0.920,-0.016)	(1.099,-5.615)	(1.064,-3.650)	(0.615,0.363)	(0.585,0.387)	0.04
PLTa2	(0.972,-0.016)	(0.963,-0.027)	(1.112,-5.980)	(1.148,-7.746)	(0.720,0.306)	(0.674,0.335)	0.005
PLTa3	(0.960,-0.025)	(0.974,-0.005)	(0.985,0.791)	(1.022,-1.228)	(0.725,0.329)	(0.690,0.345)	0.004
PLTa4	(0.877,-0.021)	(0.933,-0.005)	(1.005,-0.611)	(0.959,2.196)	(0.702,0.304)	(0.644,0.345)	0.09
PLTa5	(0.860,-0.056)	(0.901,-0.026)	(0.911,4.592)	(0.838,8.655)	(0.687,0.338)	(0.613,0.382)	0.06
PLTa6	(0.904,-0.010)	(0.919,-0.003)	(0.734,14.060)	(0.397,32.119)	(0.678,0.326)	(0.680,0.330)	0.08
PLTa7	(0.915,-0.044)	(0.998,0.035)	(1.119,-6.577)	(1.119,-6.474)	(0.736,0.311)	(0.722,0.327)	0.02
PLTa8	(0.967,-0.003)	(0.961,-0.017)	(1.027,-1.485)	(1.178,-9.515)	(0.731,0.287)	(0.705,0.313)	0.03
PLTa9	(0.933,-0.005)	(0.904,-0.031)	(1.026,-1.530)	(0.804,10.289)	(0.641,0.357)	(0.670,0.352)	0.06
PLTa10	(1.040,0.056)	(0.997,0.028)	(0.753,13.308)	(0.822,9.345)	(0.736,0.329)	(0.713,0.344)	0.04

Table 5: Same as Table 3 but for the selection cuts on both (τ, λ) and power-law \mathcal{E}_x functions.